JOURNAL OF MATERIALS SCIENCE 16 (1981) 170–188

A physical and chemical examination of an ethylene steam cracker coke and of the underlying pyrolysis tube

M. J. BENNETT, J. B. PRICE
Materials Development Division, AERE Harwell, Didcot, Oxon, UK

The physical properties, chemical composition and structure of a carbonaceous deposit formed on a radiantly heated HK40 steel tube at 920 to 930° C after ~ 50 days cracking operations in naphtha-steam have been examined. The deposit consisted of two layers. The innermost (i.e. adjacent to the tube) varied in thickness from 20 μm to 1.5 mm, and was formed by heterogeneous reactions catalysed by iron and nickel. Enhanced deposition was characterized by a higher concentration of entrapped chromium rich oxide particles, a principal source of catalytic species. The outer deposit layer was of uniform thickness, had a columnar radial and an axial layered structure, which together with the absence of any significant inorganic constituents, suggested an autocatalytic growth mechanism. The corrosion of the inner (pyrolysis) and the outer (hot box) surfaces of the underlying HK40 steel tube had similar features. The chromium rich outer scales were of variable thickness, due to the attack of certain grains, underlying which were zones denuded in carbon precipitates and intergranular silica formation. The major difference was carburization from beneath the decarburized zone at the inner surface. The processes of decarburization, carburization and of intergranular corrosion were interconnected. Carbon pick-up probably resulted from a crevice corrosion mechanism. A general reduction in the nitrogen level through the cracker tube, with enhanced denitriding at both surfaces, originated from a similar mechanism to that responsible for decarburization. The more severe denitriding at the inner surface was derived from chromium nitride conversion to the more stable chromium carbide.

1. Introduction

As a consequence of the coolants in both the Mark I and II gas cooled nuclear power plants in the United Kingdom being based upon carbon dioxide, considerable attention has been directed in the nuclear industry to the laydown of carbon onto and its movement into materials. An important principal learnt from these studies is that physical and chemical characterization of plant deposits can play a key role in directing the investigation of measures to alleviate deposition. Coke laydown on the pyrolysis tubes is an important technological problem in ethylene steam crackers, (ESC). A detailed examination of the chemical and physical properties of a particular cracker deposit has been undertaken, therefore, to demonstrate the potential value of this type of study. The corrosion of the HK40 steel tube underlying the deposit was also investigated.

2. Plant operating conditions for the material examined

The specimen, supplied by ICI Ltd, was a 100 mm long section of an HK40 steel radiantly heated cracker tube (108 mm i.d., 128 mm o.d.). On the inside of the tube there was effectively a cylinder of carbonaceous deposit (~ 1 to 2 mm thick), which had become detached. The tube had been operated for ~ 3 years on a cycle consisting of ~ 50 days cracking naphtha-steam followed by decoking to burn out the carbonaceous deposits formed. The deposit examined was therefore, laid down during the final ~ 50 day cracking period. It was derived from a region in which the gas

temperature was 820 to 830° C, while that of the underlying tube wall was 920 to 930° C. The outer tube surface had been continuous exposed to the gaseous fuel-oil combustion environment, at ~ 1 atm pressure, within the hot-box. The exact gas composition at the outer tube surface was not known but an average flue gas analysis was 9.5% carbon dioxide, 5% oxygen, < 0.1% total hydrocarbons and < 0.1% carbon monoxide. The remainder was nitrogen and water vapour. This environment would be essentially oxidizing with respect to the steel.

3. Physical and chemical examination of the carbonaceous deposit

3.1. Introduction

The two surfaces of the deposit were visually different. The outer surface (i.e. originally the interface with the gas) had an undulating topography, a shiny appearance and the material was coherent. The inner surface (i.e. the interface with the cracker tube) in contrast was rougher, had a matt appearance and consisted of friable material having a fine structure. The two layered structure was confirmed by subsequent examination. To enable bulk measurements on the outer, thicker, layer alone, the inner layer was removed by abrasion on silicon carbide paper. Since the inner layer was non-uniform in thickness, the position at which abrasion was discontinued had to be somewhat arbitrarily decided by the surface appearance alone.

3.2. Physical measurements

The surface area of the complete deposit was determined, by the BET method, from the measurement of the adsorption of xenon at 78 K. The value obtained was 1350 $cm^2\ g^{-1}$, which in terms of the geometric surface area gave an average roughness factor of 193. The bulk and apparent densities of the complete deposit and the outer layer were determined by immersion in mercury and helium respectively (Table I) and they indicated that both contained 11 to 12% open porosity. Although the deposit was graphitic in structure (Section 3.5), its density was lower than that of graphite (2.25 $g\,cm^{-3}$) suggesting that the deposit also contained ~ 12% closed porosity. No gas permeability through the outer layer was measured with nitrogen as the viscous flow coefficient was smaller than the minimum measureable ($< 1 \times 10^{-12}$ cm^2).

3.3. Chemical analysis

The chemical and spectrographic analyses of the complete deposit and of the outer layer are given in Table II. The iron, chromium and nickel contents of the deposit were associated primarily with the inner layer and were significant. The hydrogen, oxygen, nitrogen, sulphur and silicon contents of the complete deposit and of the outer layer were comparable. The oxygen contents were higher than could be accounted for by association with the hydrogen as adsorbed water. This would suggest rather that both elements were chemically bound with carbon and/or another element within the deposit, as sulphur would also appear to be.

3.4. X-ray photoelectron spectroscopy analysis of metallic impurity distribution in outer deposit layer

X-ray photoelectron spectroscopy (XPS) analyses of the outermost deposit surface and of the inner surface of an abraded specimen were similar (Table III). They did not indicate any iron concentration within either the $\leqslant 0.5\,\mu m$ thick outer surface layer or alternatively the deposit nearer to the steel to suggest a concentration gradient across the deposit. It would appear rather that any potential catalytic impurities were distributed randomly throughout the outer layer. The high oxygen and nitrogen levels on the original surfaces probably represented adsorbed air.

3.5. X-ray diffraction analysis

Both the cracker tube and gas interfaces of the deposit were examined with an X-ray diffractometer, using CuKα radiation. The inner deposit layer was shown to consist primarily of graphite with two degrees of crystallinity, as broad bands were obtained for the (002) and (101) planes having d values of 3.35 and 3.52 Å respectively. A weak Fe_3O_4 pattern was also observed, together with a single unidentified weak line. The

TABLE I Densities of the complete deposit and outer layer

	Bulk density ($g\,cm^{-3}$)	Apparent density ($g\,cm^{-3}$)	Open porosity (%)
Complete Deposit	1.62	1.87	11
Outer Layer	1.61	1.82	12

TABLE II Chemical analysis of the total deposit and of the outer layer

Material	C	H	O	N	S	Si	Fe	Cr	Ni	W	Other elements
Total deposit	95*	0.15*	0.3*	350	65	200	0.7*	0.15*	0.1*	200 500	Al 70, Cl 80, Ca 50, Cu 10, Mn 50, Co 100, Mo 5, V 7, Zr 10. Remaining elements less than detection limits.
Outer layer	> 99*	0.22*	0.2*	200	70	300	200	50	50	< 50	Al 70, Ca 70, Cu < 5, Mn < 5, Co 30, Mo < 5, V < 5, Zr < 10. Remaining elements less than the detection limits.

* wt %, remaining values in ppm.

corresponding examination of the outer gas interface of the deposit gave a weak graphite pattern, with only a solitary broad band with $d = 3.5$ Å.

3.6. High voltage electron microscopy

Fragments of both the inner and outer layers were thinned initially by standard metallographic polishing techniques. Each side was abraded in succession. The outer layer was reduced to the required thickness (0.03 mm) directly by this procedure. However, the inner layer material started to break up when its thickness was 0.3 mm. The remaining surplus material was removed by vibratory polishing a mounted specimen placed face downwards in a slurry of gamma-alumina and water. When its thickness had been reduced to 0.03 mm, it was etched with 5 keV argon ion beams directed at an angle of incidence of about 30° on to both specimen surfaces. The material was eroded until a small hole appeared in the specimen.

The transmission electron microscopy (TEM) examination was carried out with an AEI 1 MeV microscope. The outer layer consisted of a homogeneous array of randomly orientated crystallites, with a small crystallite size < 30 Å (Fig. 1a and b) and with the (002), (011) and (112) planes reflecting (Fig. 1c, Table IV). Within this matrix were unidentified inclusions of various shapes and sizes, the largest being ~ 3 μm diameter and the finest ~ 50 Å diameter. The inner layer was composed of agglomerates (0.05 to 0.5 μm) of crystallites (< 50 Å diameter) interspaced with pores of a comparable size to the agglomerates (Fig. 1d and e). The diffraction pattern from this material was similar to that from the outer layer, (Table IV) except that the rings were sharper and better defined due to the larger crystallite size (Fig. 1f). Few if any inclusions were visible in the inner layer section examined.

3.7. Scanning electron microscopy

The topography of the inner and outer deposit surfaces and of a cross-section through the deposit were examined in a scanning electron microscope. Qualitative chemical analyses were obtained with an EDAX dispersive X-ray analyser. Two types of deposit structure were clearly distinguishable. The inner layer at the steel interface essentially consisted of nodules of interwoven filaments

TABLE III XPS analysis (at %) of outer and abraded deposit surfaces

Element	Outer surface				Abraded surface		
	Original surface	100 Å removed	1100 Å removed	0.5 μm removed	Original surface	100 Å removed	1100 Å removed
C	77.6	95.9	97.0	96.6	80.8	97.2	97.3
O	16.5	3.4	2.9	3.4	14.6	1.9	2.6
Fe	~ 0.06	0.12	0.10	0.07	0.08	0.12	~ 0.05
Si	0.9	0.2	–	–	1.9	0.25	–
S	2.2	0.4	Trace	–	0.5	0.2	–
N	2.2	–	–	–	1.8	~ 0.3	–
Cl	–	–	–	–	0.3	–	–
Na	0.5	–	–	–	–	–	–

Analyses of ~ 0.3 cm² surface to 20 Å mean depth.
Limits of detection of Fe, Ni and Cr ~ 0.05 at %.

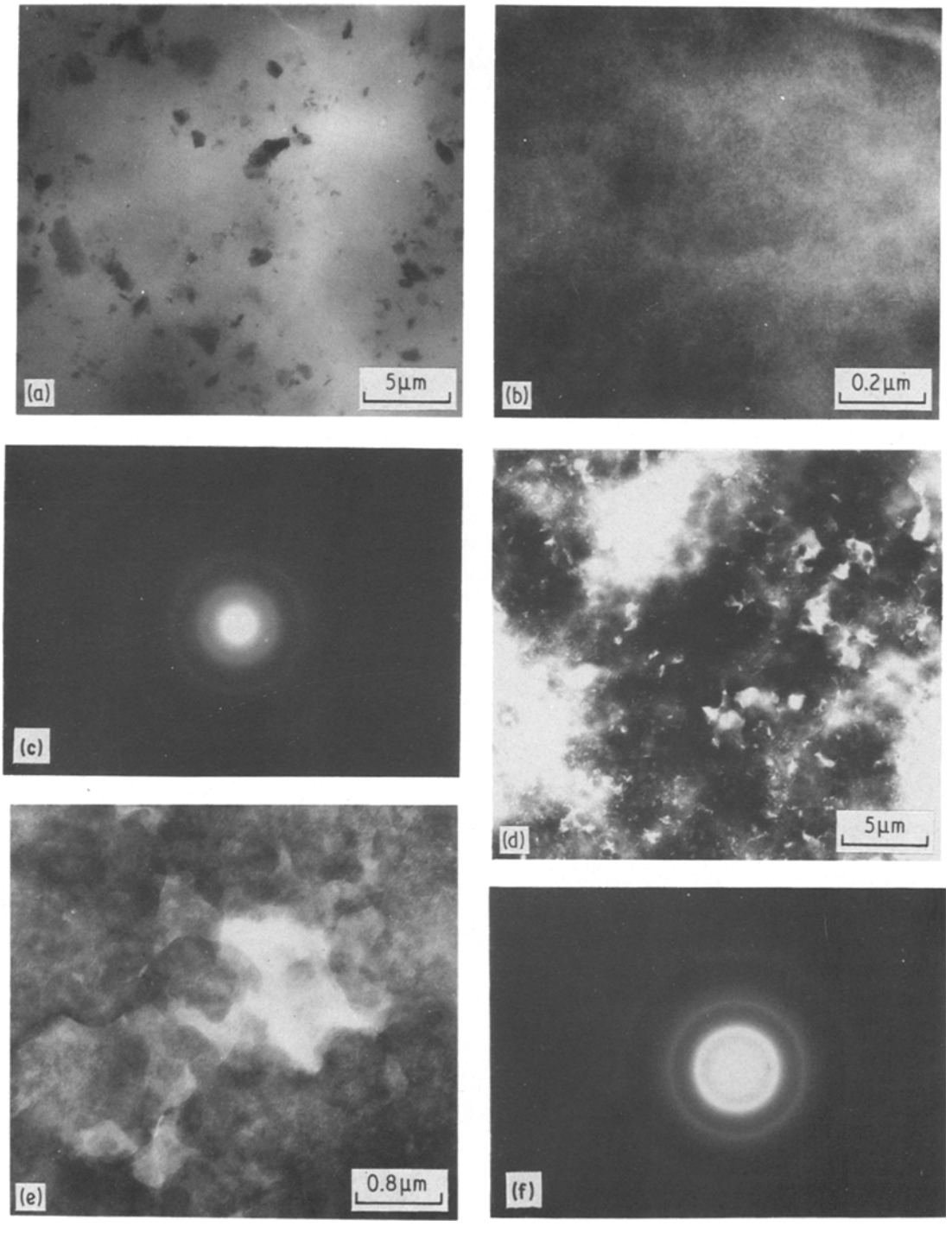

Figure 1 (a) and (b) are transmission electron micrographs of the deposit (outer layer), (c) is an electron diffraction pattern of the outer layer with a camera length of 484 cm, (d) and (e) are transmission electron micrographs of the deposit (inner layer), and (f) is an electron diffraction pattern of the inner layer with a camera focal length of 484 cm.

(Fig. 2a and b), which could be up to 2–5 μm thick. Within this layer were embedded angular shaped particles of varying sizes ($<$ 2–25 μm), which contained chromium and to a lesser extent, iron and nickel. Other elements (aluminium, silicon, potassium, chlorine and sulphur) were also present at smaller concentrations. The thicker outer layer was coherent in structure and its gas

TABLE IV Comparison between the interplanar spacings of graphite, and of the inner and outer ESC deposit layers

Graphite		ESC deposit	
Plane	Spacing (Å)	Outer layer (Å)	Inner layer (Å)
001	6.71		
002	3.25	3.41	3.30
003	2.23		
010	2.13		
011	2.03	2.05	2.05
012	1.80		
103	1.54		
112	1.15	1.17	1.16
113	1.08		
021	1.05		

interface had a tiered topography (Fig. 2c). Small (~ 2 μm diameter) particles randomly dispersed on the outer surface contained the same variety of elements noted above. Less than one in twenty particles contained either iron or nickel. The number of particles per cm^2 surface area was smaller than on the inner deposit interface and they appeared to be on, rather than embedded in, the outer surface. They could have arisen from post-cracking handling operations rather than from in-plant service. The topography of the cross-section across the deposit was typical of a fracture surface through this type of material. At localized regions the inner layer apparently protruded into the outer deposit (Fig. 2d). The presence of discrete chromium-rich areas within these regions, which also contained iron and nickel, suggested that these particles were embedded at least throughout the inner layer. Two small areas of the deposit cross-section nearest the tube interface were covered with dendrites of potassium chloride (Fig. 2e and f).

3.8. Optical metallography and electron probe microanalysis

Deposit cross-sections were examined metallographically and analysed using a CAMEBAX EPMA. The latter data were displayed in two ways, as a series either of elemental X-ray images for the same area or of traces of the X-ray intensity variation for each element across the same

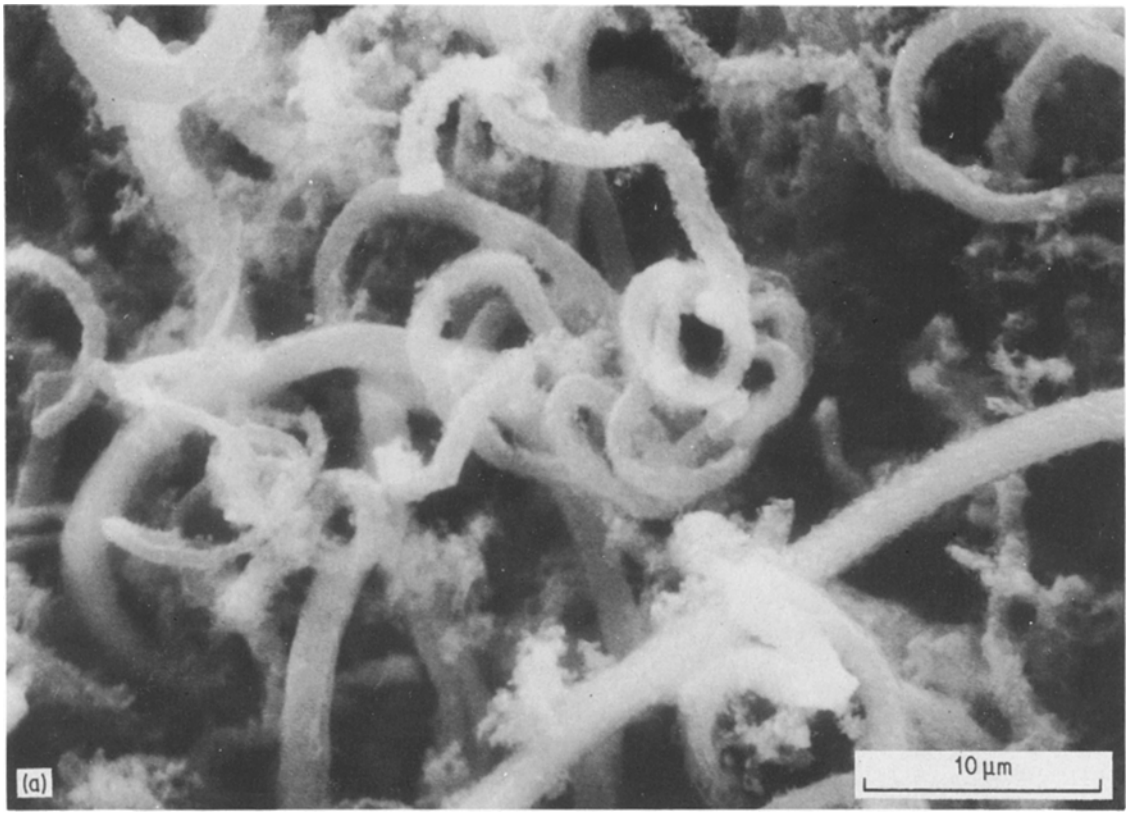

Figure 2 Scanning electron micrographs of (a) the inner surface, (b) an edge view of the inner layer at tube interface, (c) the outer surface, (d) a deposit cross-section near tube interface, (e) a deposit cross-section showing KCl dendrites near tube interface and (f) KCl dendrites.

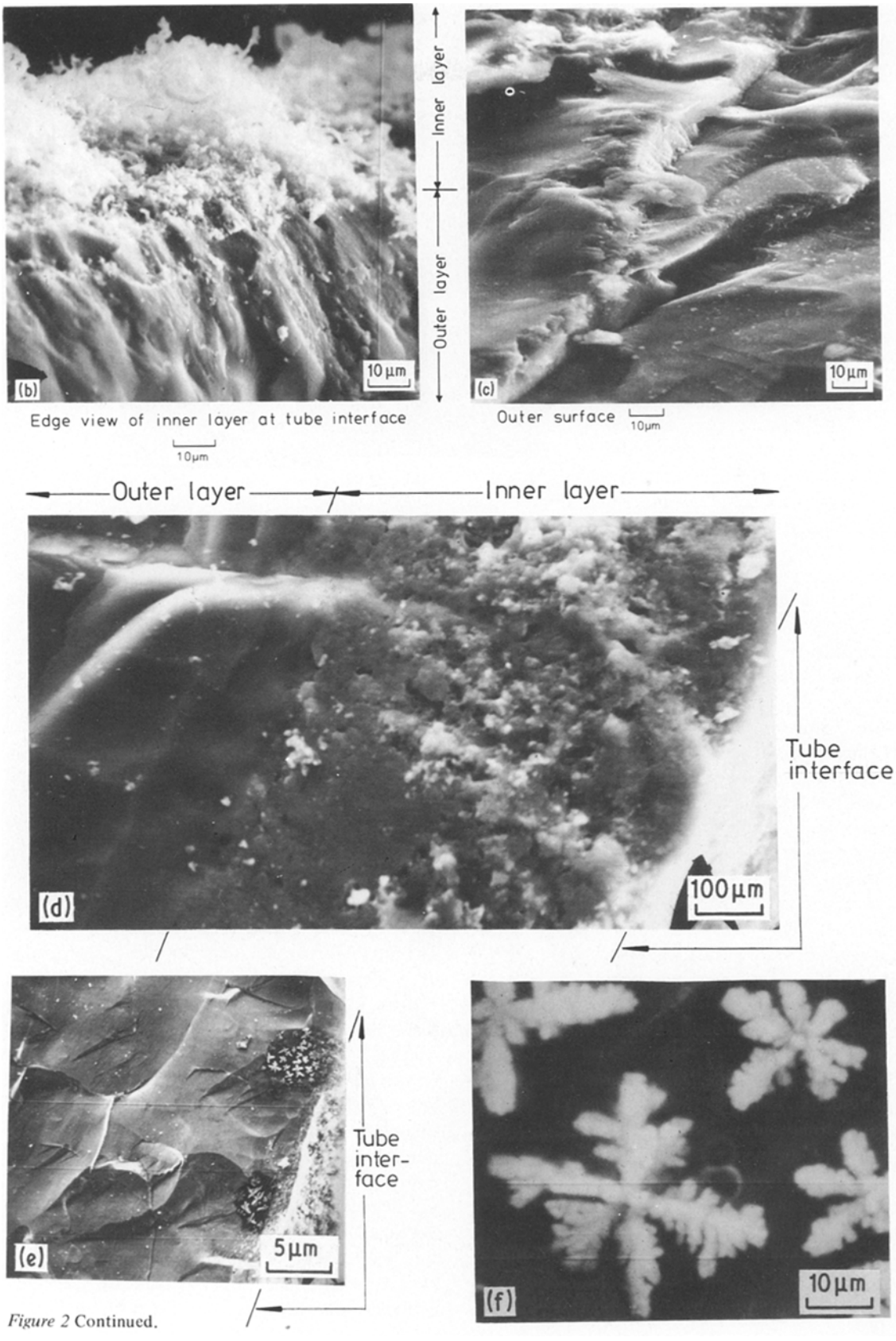

Figure 2 Continued.

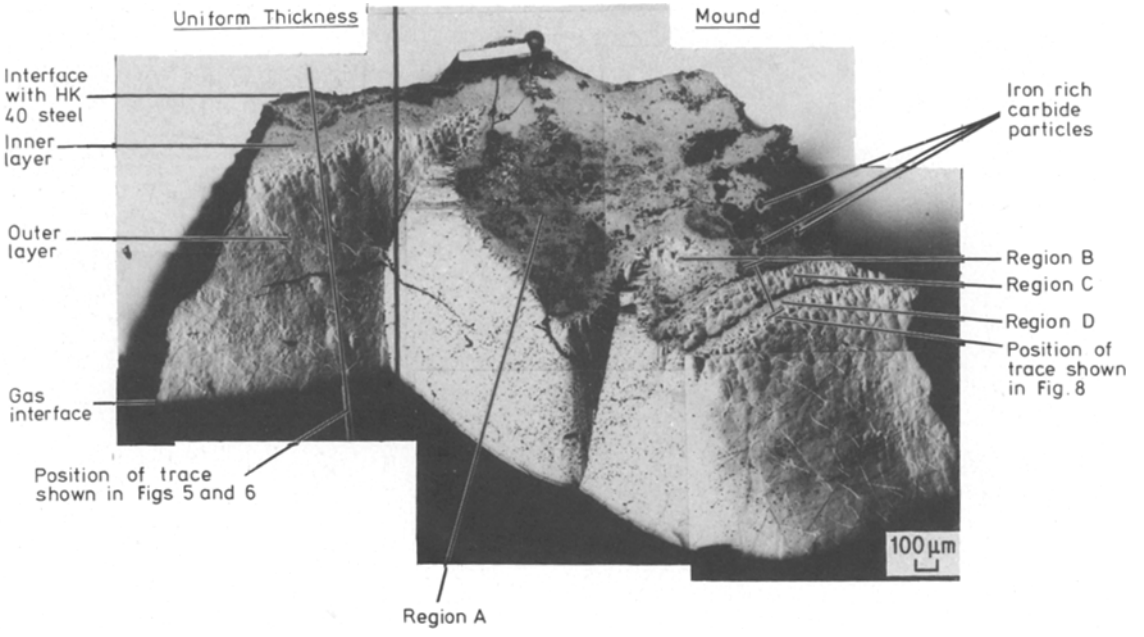

Figure 3 Metallographic section through uniform and mound deposit sections (polarized light).

traverse, unless stated otherwise. In the latter, the limits of detection or lowest concentration are indicated.

In a cross-section representative of uniform thickness deposit between the mounds, two layers were clearly distinguishable (Fig. 3). Throughout the inner porous layer iron, and to a lesser extent nickel, were dispersed randomly (Figs 4a and 5). Their concentrations were higher within a band nearest to the cracker tube interface, which was also characterized by the presence of discrete oxide particles, whose principal metallic constituent was chromium but which also contained iron (Fig. 4b to f). The inner layer also contained small concentrations of potassium, chlorine and sulphur. The thicker outer layer was completely different, as it interacted with polarized light to show an ordered growth structure (Fig. 3). The extent of the closed porosity was smaller than that in the inner layer, while there were no entrapped oxide particles. EPMA traverses across the outer layer (Figs. 5 and 6) indicated that the nickel, iron, chlorine, potassium and sulphur levels were less than the detection limits.

Although the section through a mound appeared to be more complicated it still essentially consisted of two principal layers. The increase in overall deposit thickness was attributable entirely to enhanced inner layer growth, as the thickness of the enveloping outer coherent layer was comparable to that between the mounds. The main feature of the thicker inner layer was the higher density of chromium rich oxide particles embedded within the iron and nickel bearing deposit matrix (e.g. in region A, Fig. 3). The overall similarity of the analyses of the principal metallic constituents of these particles within the uniform and mound deposit sections (Table V) would suggest that they probably originated from the same source. A limited number of another type of iron rich carbide particle were apparent (Fig. 7), which also contained small quantities of nickel, oxygen, phosphorus and discretely dispersed chromium. The metallic carbide particles were surrounded by a deposit shell of variable thickness, having a more coherent structure with lower porosity than the surrounding deposit matrix. A final feature of the mound section was that at two regions (B and C, Fig. 3) growth of the structurally ordered deposit had been interrupted by metal catalysed deposition (e.g. region D, Fig. 3). The ordered deposit in region C was essentially metal-free (Fig. 8). Discrete iron rich particles (1 to 5 μm diameter) were located both at the interfacial boundary and also to a depth of 20 μm within this $\sim$40 μm thick region D, which had an inner layer type structure. This was then superceded by coherent outer layer growth. The structural orien-

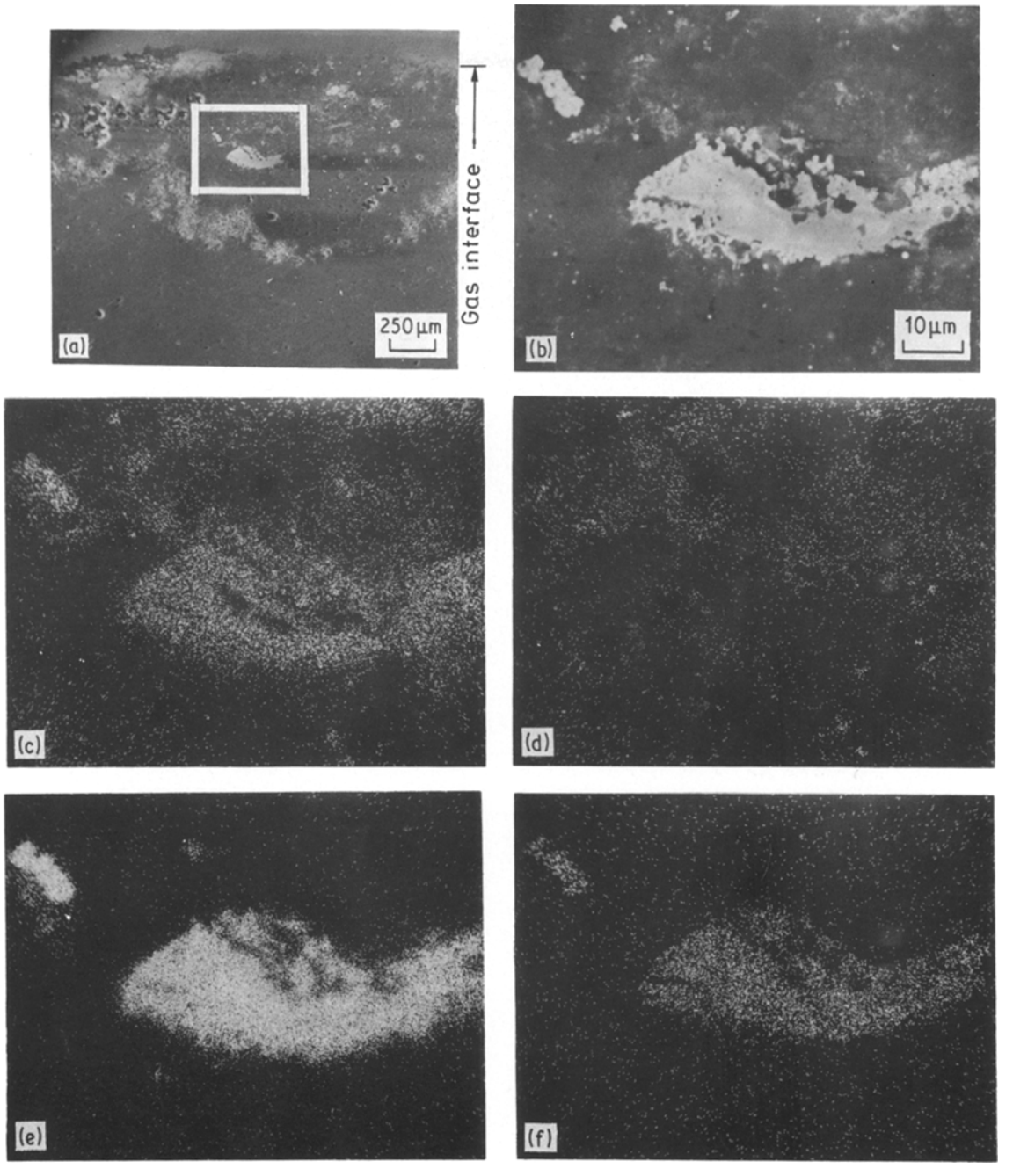

Figure 4 EPMA of inner deposit layer (a) electron image, (b) enlarged section of (a), (c) Fe X-ray image, (d) Ni X-ray image, (e) Cr X-ray image and (f) O X-ray image.

tation of the outer layer varied, in part attributable to variations in inner layer thickness (Figs. 3 and 9). The section through a second fairly uniform thickness deposit clearly indicates an axial layered pattern parallel to gas interface and radial multinucleated columnar growth structure (Fig. 9).

Consideration of the implications of these results regarding the possible mechanisms of deposit laydown will be given in Section 5, as the corresponding data from the examination of the HK40 steel cracker tube reported in the next section are relevant to this interpretation.

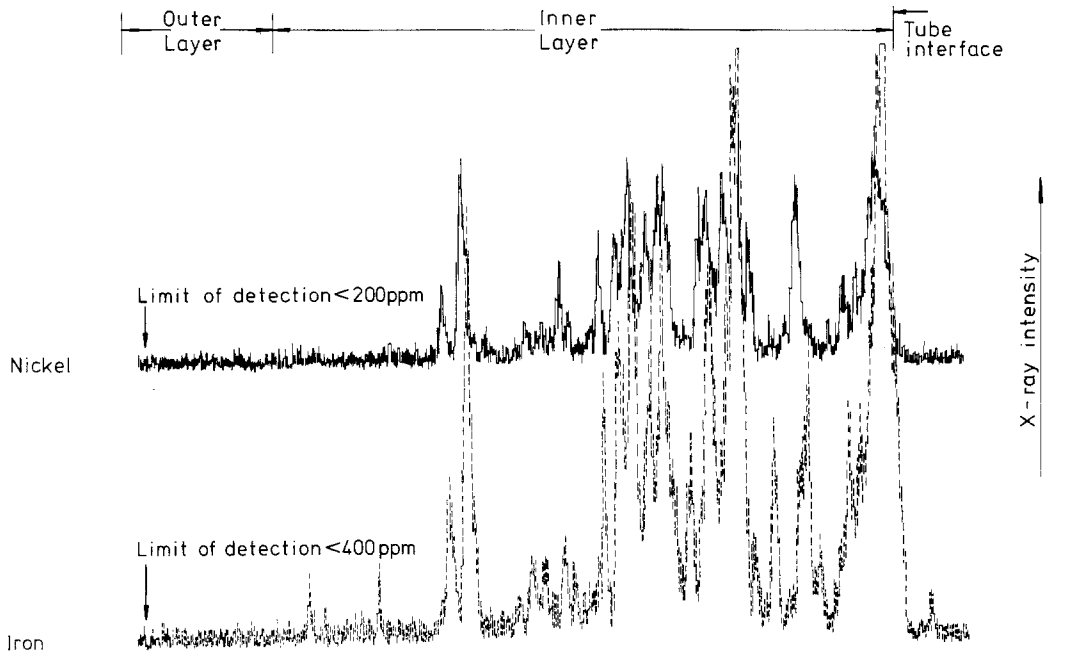

Figure 5 Variation of iron and nickel contents through the deposit to a depth of 512 μm from the tube interface (position of trace shown in Fig. 3).

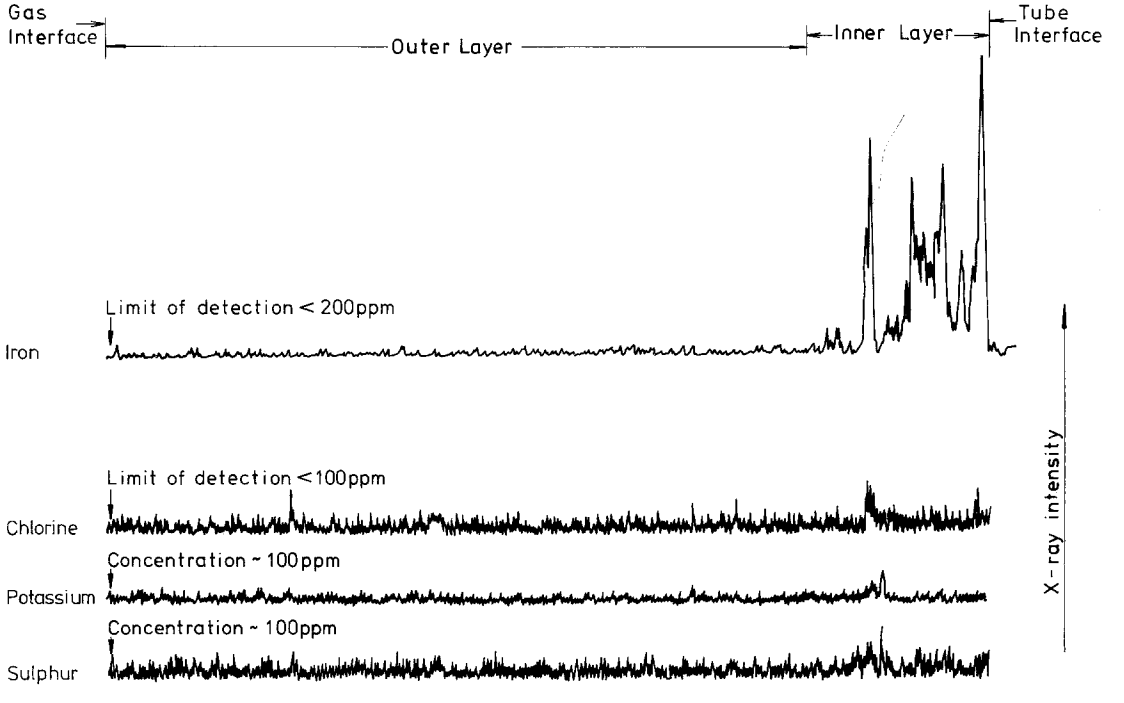

Figure 6 Variation of iron, sulphur, chlorine and potassium concentrations across uniform thickness deposit section (position of trace shown in Fig. 3).

TABLE V Analysis (wt %) of the major metallic constituents of chromium-rich oxide type particles within the inner layer of uniform and mound deposit sections

Section	Cr	Fe	Ni	Si
Uniform section	48.3	18.7	3.2	2.0
	42.3	21.7	1.9	2.2
Mound section	54.6	11.2	3.4	1.5
	60.4	5.5	< 0.1	0.9
	52.5	14.3	0.5	1.3
	58.2	6.4	3.5	4.5

4. Examination of the HK40 steel cracker tube

4.1. Introduction

The HK40 steel cracker tube on which the deposit was formed was probably cast material with a machined bore. For comparison purposes a section of a similar tube, in the as-fabricated condition was supplied by ICI Ltd. The analysis of this material is given in Table VI.

4.2. Optical metallography

The form of the attack of both the inner (i.e. interface with deposit) and outer (i.e. hot-box) surfaces of the cracker tube was comparable, other than in one important aspect (Fig. 10). The principal common features were an outer, cracked, adherent scale of variable thickness, due primarily to the complete attack of certain surface grains, intergranular oxidation and a region of unattacked steel denuded of carbide precipitates beneath the outer scale. The maximum scale thickness at both surfaces was similar, while the depths of the intergranular oxidation were slightly (30%) smaller at the inner surface (Table VII). The thickness of the carbide denuded zone at the inner surface was comparable to that of intergranular oxidation, while by comparison, at the outer surface the denuded zone was slightly thicker. The major difference between the form of the attack of the two tube surfaces was extensive carburization beneath the decarburized zone at the inner tube surface. There was a continuous network of carbide stringers at the grain boundaries and massive carbide precipitation within the grains. The precipitate density decreased with increasing depth into the steel.

4.3. Electron probe microanalysis

At both surfaces the continuous scale was predominantly chromic oxide (Fig. 11). Some iron and manganese were present near the gas interface with the former being depleted and the latter enriched, compared with the levels in the alloys. Nickel was almost completely absent. Internal oxidation of a grain was associated with chromium enrichment above that in the bulk steel. Nickel, possibly in the metallic state on account of the gas composition, was concentrated at discrete regions near the inner oxide–steel interface and its level then decreased across the grain to the gas interface. The iron concentration also decreased across the grain from the oxide–steel interface. Manganese was enriched in localized regions, particularly near the gas interface. Beneath the oxide, for a depth of 100 to 125 μm at the inner surface and greater than that scanned ($\sim$ 40 μm) at the outer surface, chromium was depleted slightly, but its concentration increased from the oxide–steel interface. These regions would appear to coincide with the decarburized zones observed metallographically. The intergranular oxide was almost entirely silica. The extensive precipitates formed beneath the internal oxidation at the inner surface were of chromium carbide.

4.4. Nuclear microprobe measurement of carbon and nitrogen profiles

Cross-sections of the HK40 tubes, in both the as-fabricated condition as well as from the cracker, were mounted in Woods metal, a carbon-free mounting medium and were polished with an alumina abrasive. The analytical method for carbon [1] was based upon irradiation with 1.3 MeV deuterons and measurements of the protons emitted by the $^{12}C(d, p)^{13}C$ reaction. The carbon contents were obtained by calibration against steel standards. The location of the ion beam on the specimens was established by simultaneous measurements of the emitted iron, chromium and nickel X-rays.

The as-fabricated steel tube was examined to 500 μm depth from each surface at a spatial resolution of 25 μm. There were large short-range variations in the carbon concentrations with the mean value near to both surfaces being 0.33%, which was in near agreement with the average bulk chemical analysis (0.36%). The surface regions of the exposed tube were examined at a spatial resolution of 50 μm (Fig. 12). At the outer surface the carbon concentration was depleted markedly to a depth of about 200 μm before rising to approximately the bulk level; the average of the 14 points from 225 to 875 μm was 0.29%. The

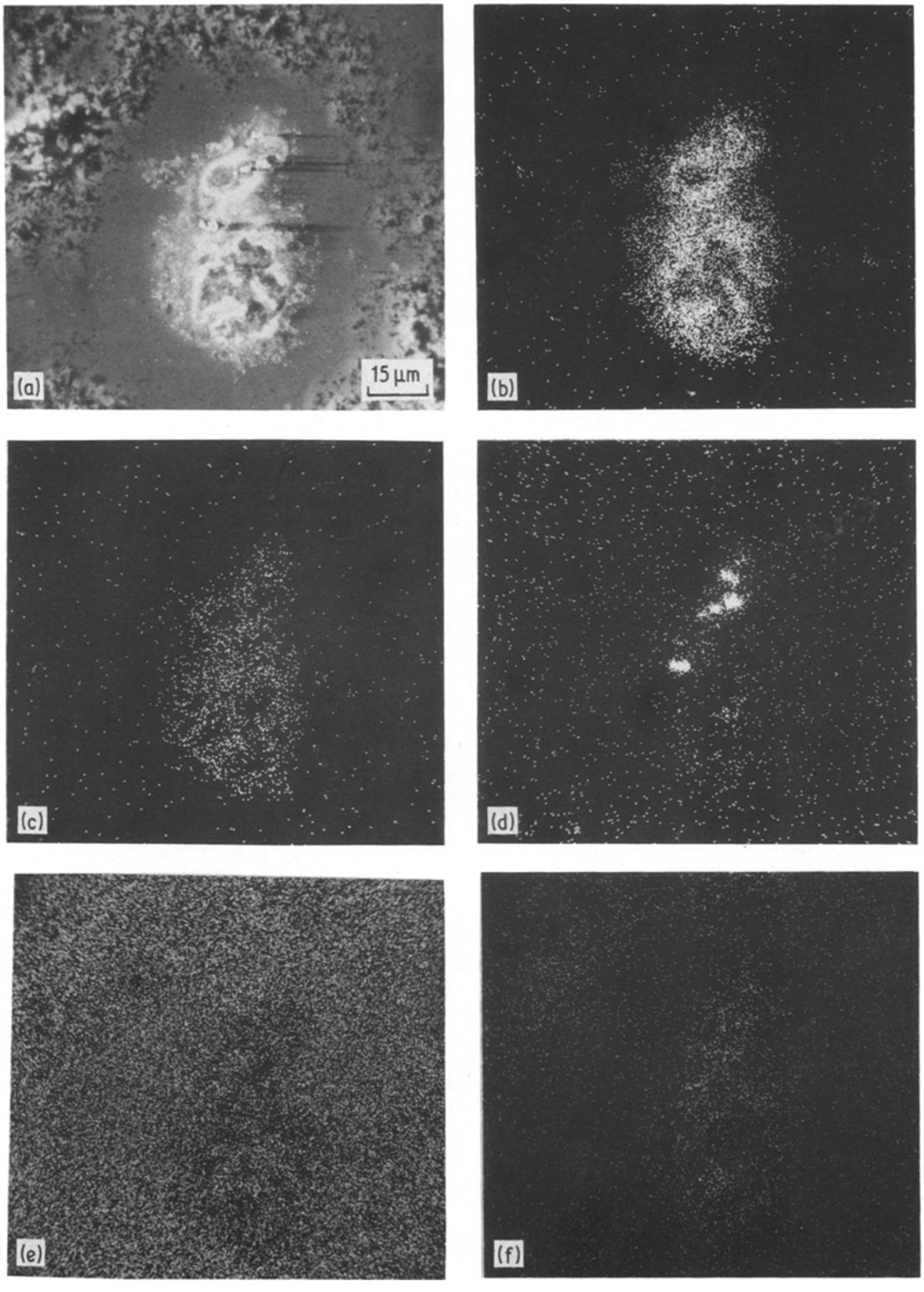

Figure 7 EPMA of iron-rich particles in inner layer of deposit mounds (a) electron image, (b) Fe X-ray image, (c) Ni X-ray image, (d) Cr X-ray image, (e) C X-ray image and (f) O X-ray image.

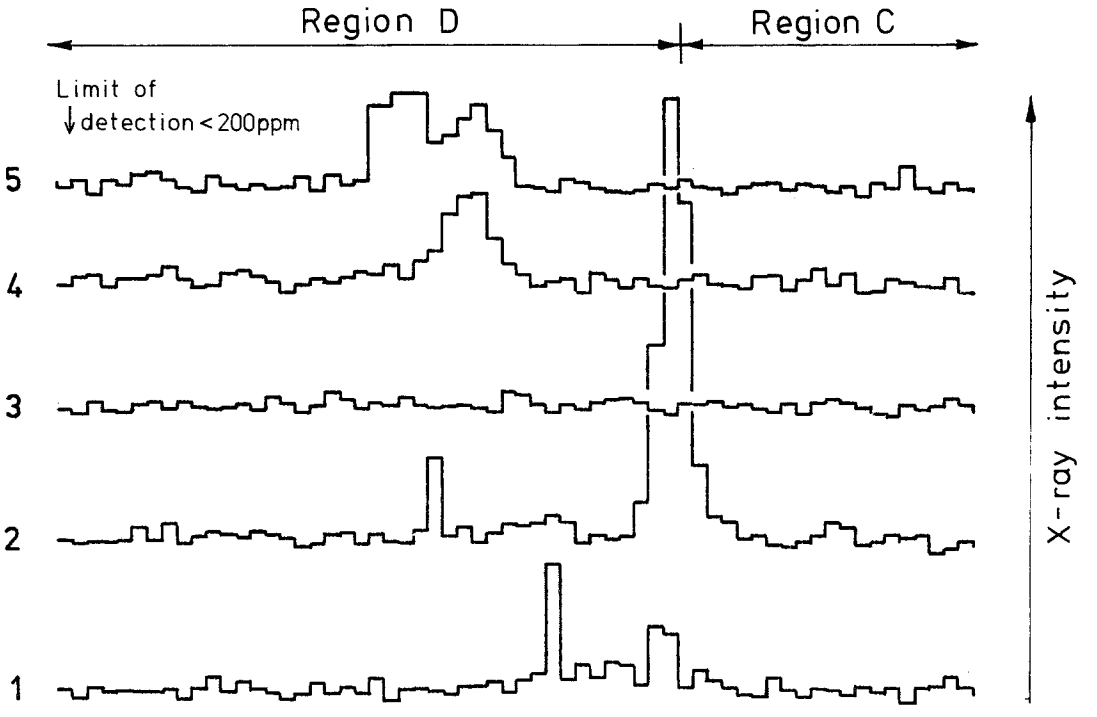

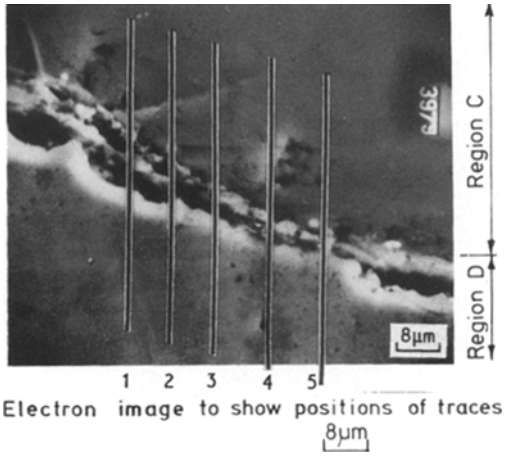

Figure 8 Variation of iron concentrations from region C to region D. The micrograph is an electron image showing the positions of the traces.

concurrent X-ray spectrum variation confirmed EPMA observations that the chromium concentration decreased simultaneously with the carbon. At the inner surface carbon and chromium were depleted at a depth of 25 μm but carbon was picked up at 125 μm. The carbon concentration increased to over 0.7% on average between 125 and 475 μm from the surface but then fell slowly to 0.5% at 2000 μm. The carbon profiles were consistent with the metallographic observations.

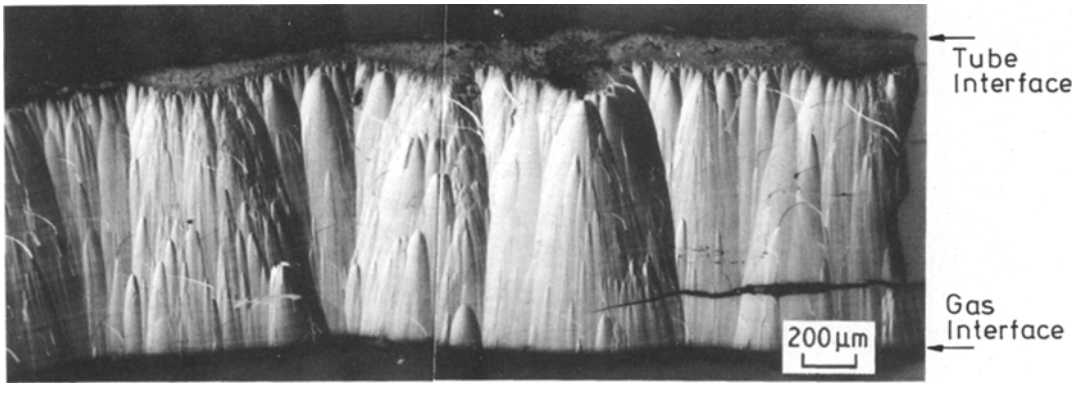

Figure 9 Metallographic section through uniform deposit section (polarized light).

TABLE VI Analysis of HK40 steel (wt %)

Cr	Ni	Mn	Si	Mo	Nb	Sn	Al	Ti	C	S	P
25.2	18.1	1.50	1.20	0.54	0.06	0.02	< 0.01	< 0.01	0.36	0.024	0.02

The nitrogen profiles across both as-fabricated and exposed tubes were also examined using the nuclear microprobe [2]. The average nitrogen content of the archive material was 0.19%, although the concentration varied on a short range basis, with the maximum and minimum individual values being 0.32% and 0.13% (Fig. 13). There was a general reduction in the nitrogen level of the exposed tube to ~ 0.12% and more severe denitriding at both the outer and particularly the inner surface. The nitrogen levels decreased from the maximum bulk concentration to that at the surface (100 to 200 ppm) more sharply at the outer surface over a depth of ~ 400 μm than at the inner surface, where the depth of the affected zone was ~ 5 mm.

4.5. Discussion

Two factors must be borne in mind when considering the extents of attack of the HK40 steel surfaces. Firstly, metallographic examination established only the magnitude of the oxide scale adhering to the steel and this would only be a measure of the total corrosion if no oxide had spalled. The extent of this could not be ascertained. Secondly, the outer surface was exposed to, and thus was corroded by, an oxidizing environment throughout the tube life. By contrast the inner tube surface was only oxidized for a proportion of this period, as coke formation would have restricted gas access. This cannot be defined precisely but it was probably during the initial plant start-up, successive decoking operations and possibly the early stages of each cracking cycle before the onset of massive coking. The differences between the respective exposure periods of the two surfaces had no significant influence upon the extent of the outer scale formation but could have been responsible for the

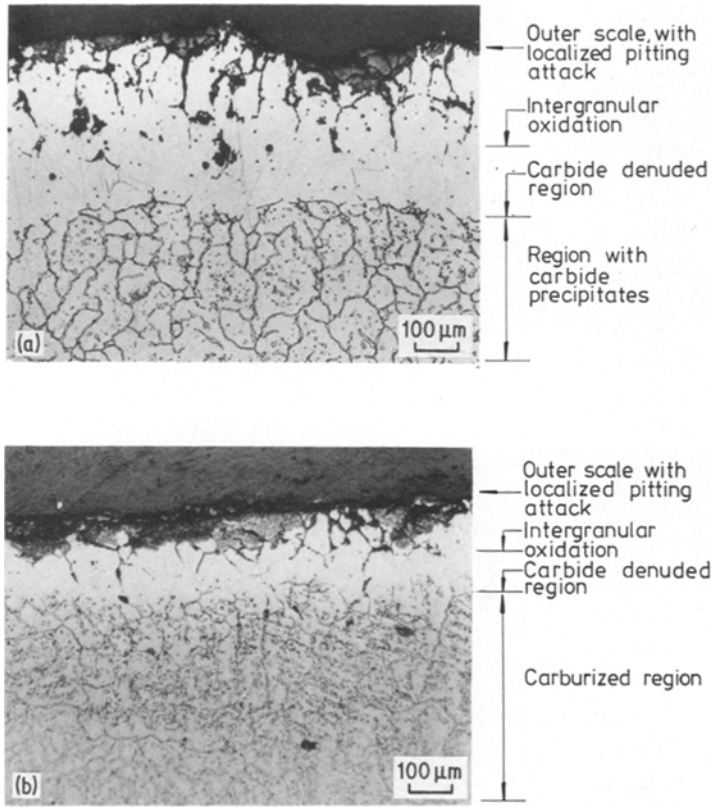

Figure 10 Optical micrographs of the inner and outer surfaces of HK40 steel cracker tube, etched in 10% oxalic acid. (a) outer (hot-box) surface and (b) inner surface underlying carbonaceous deposit.

TABLE VII Comparison between the extents of attack of the inner and outer HK40 cracker tube surfaces

Surface	Maximum thickness (μm)		
	Outer scale	Intergranular oxidation	Carbide denuded region
Inner	80	230	180
Outer	70	300	400

30% reduction in depth of intergranular oxidation at the inner surface.

There were no apparent differences in the composition of the oxidation products at the two surfaces, and in particular the elemental variation across the outer scale, which could be attributable to the involvement of steel constituents in the formation of carbonaceous deposits at the inner surface. However, its possibility cannot be eliminated, as the amounts of steel constituents involved would be small. Chromium released from the carbides was probably involved in oxide film formation, as endorsed by the observed diffusion gradient in the underlying steel.

Intergranular attack of alloys has often involved the oxidation of a specific component, in this instance, silicon. It occured by separate processes from that responsible for outer scale formation and probably was also initiated at the onset of the exposure. It was controlled by the diffusion to the site of oxidation either of the oxidant in a gaseous or ionic form or of the silicon selectively oxidized. At both the inner and outer cracker tube surfaces the respective depths of the intergranular oxidation and of the carbide denuded zone were similar. At the inner surface only this corresponded also to the position for the onset of carburization of the underlying steel. This correlation would suggest that intergranular processes were involved in the decomposition of the carbide particles and movement of chromium to form the outer scale, as well as the localized preferential oxidation of silicon. Both processes could have opened up the grain boundaries and facilitated gas access to the steel interior. The carburization of this steel probably arose from a crevice-type corrosion mechanism. The gas diffusing through cracks and pores in the oxide would have been that within the cracker and comprised of both oxidizing (water vapour) as well as potential carburizing (hydrocarbon) constituents. Removal of the oxidants to form silica and chromic oxide would have left essentially hydrocarbons towards the base of the porous region. These would have been decomposed, possibly catalytically, to carbon, which then would have diffused into the underlying alloy, eventually to be precipitated as chromium carbide. This would seem to be a more logical explanation for the carburization of this particular steel than any advanced previously based on the carbonaceous deposit being the carbon source [3, 4]. Direct reaction between the deposit and the steel would have been prevented by the intervening coherent oxide film. A similar three-way correlation between intergranular oxidation, sub-scale decarburization and carburization has been observed recently on the nimonic alloy PE16, after oxidation in carbon dioxide at 700 to 800° C [5]. It would appear that this could be a general phenomenon.

Nitrogen was probably present in the steel originally as chromium nitride. One mechanism for denitriding was probably similar to that responsible for decarburization as supported by the comparable depths ($\sim$ 400 μm) of the carbide and nitride denuded zones at the outer surface. At the inner surface the depth of denitriding was considerably greater and another mechanism was involved. This was probably associated with the carburization within the same region and resulted from the conversion of chromium nitride to the more stable chromium carbide.

5. Mechanism of deposit formation

It is well known that iron and nickel catalyse hydrocarbon decomposition to form carbonaceous deposits characterized by a filamentary structure, with the catalytic element being located at either the tip of the base of the filament or along its length [6–8]. The inner layer had similar characteristics, and consequently this undoubtedly also derived from heterogeneous reactions involving iron primarily but also probably nickel. The other constituent of the inner layer, chromium oxide, was unlikely to have been involved directly in filament growth. The surface exposed initially to the cracking environment, and on which the deposit was first formed, was that resulting from the last decoking operation, the outer surface of the oxide film formed on the HK40 steel. There would appear, therefore, to be three possible sources of the catalytic elements. The first was the oxide film on the HK40 steel, while the second would be any inorganic oxide residue remaining on the tube surface from the oxidation

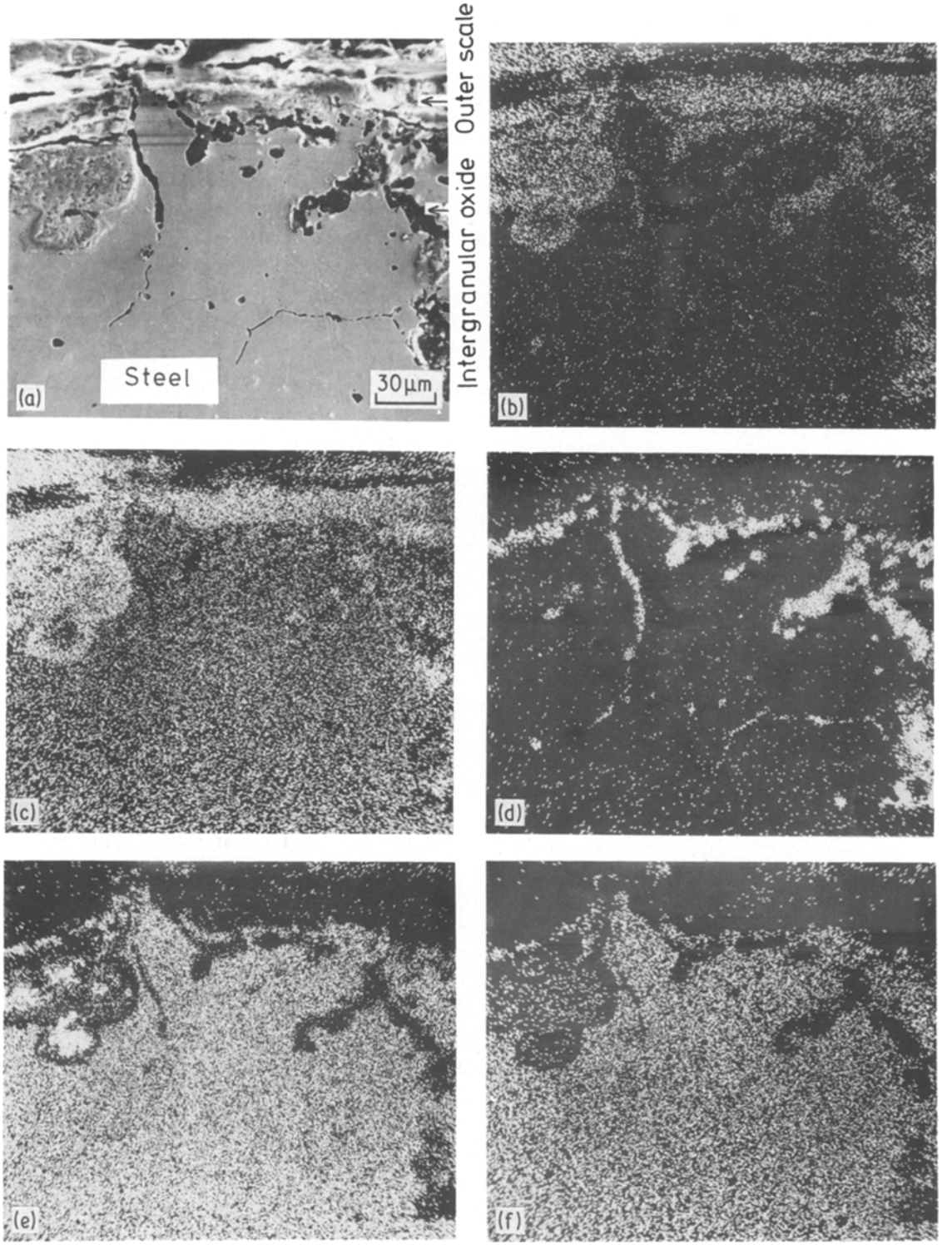

Figure 11 EPMA of outer surface of HK40 steel cracker tube (a) electron image, (b) O X-ray image, (c) Cr X-ray image, (d) Si X-ray image, (e) Ni X-ray image and (f) Fe X-ray image.

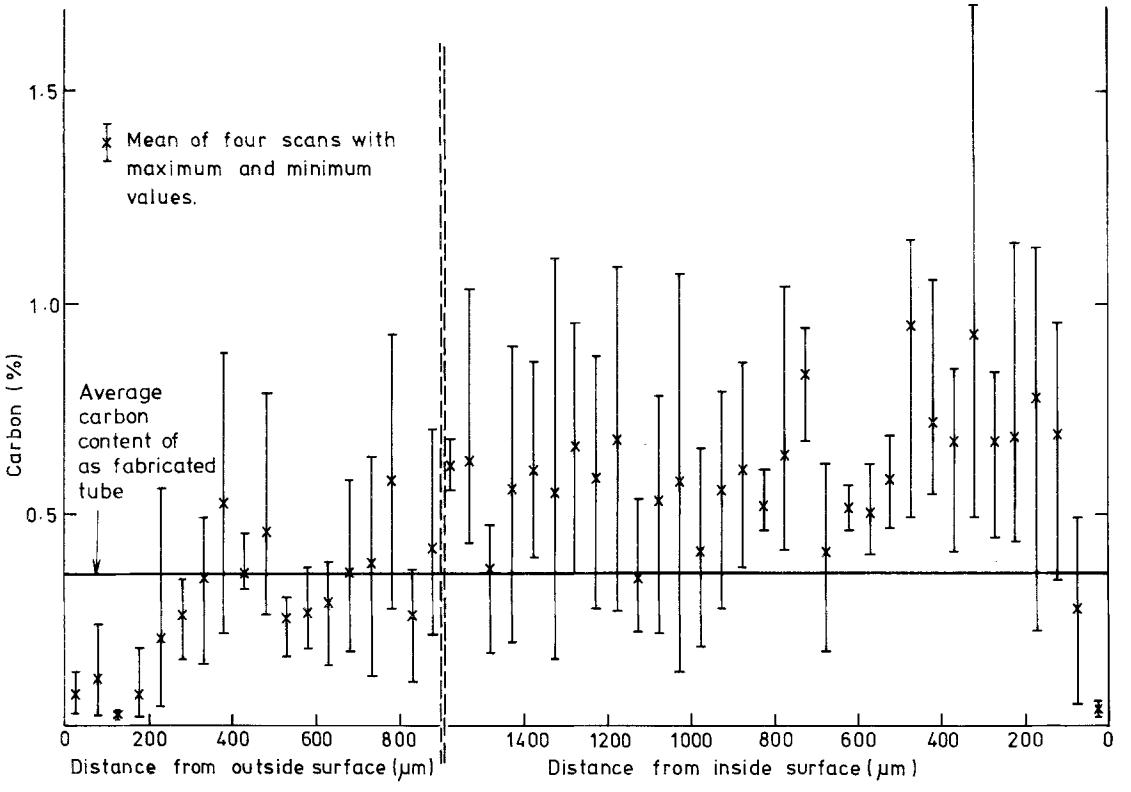

Figure 12 Carbon profiles at the inner and the outer surfaces of an HK40 steel cracker tube after service.

of the previous deposit, if this had neither spalled nor been eroded. The third possibility could be oxide dust, which had spalled from a component upstream and which had been trapped on the growing deposit. With regard to the first possible source, the composition of the oxide films on the HK40 steel would not appear to favour its direct involvement in deposit formation. It was chromium-rich, while the iron and nickel levels were considerably smaller than in the basic steel, and decreased from the oxide–steel to the oxide–gas interface. A more probable mechanism could have been that some of the Fe and Ni cations diffusing through the oxide scale and involved in its continuing growth, instead nucleated as catalytic deposition sites.

Turning to the second source, based on observations from the decomposition of acetone on a 20% Cr/25% Ni/niobium stabilized austenitic steel [9], any inorganic oxide residue from deposit burn-off remaining on the inner tube surface on the return to cracking operations could have promoted deposit formation. The third possible source of the catalytic elements, spalled oxide, would appear also to have been primarily responsible for the localized regions of enhanced growth of the inner layer and the temporary reversion in the outer layer from ordered to metal catalysed deposition. Two types of particle were embedded in the deposit. The chromium-rich oxide particles undoubtedly had provided an additional source of iron and nickel catalytic species. There were also a limited number of micron-size carbide particles, apparently as kernels within an outer carbon shell, suggesting that the shell might have grown during the transit of the particles through the gas phase and thus before the particles were trapped on the tube surface. These coated particles then appeared to have been engulfed *in situ* by the deposit, rather than having been involved in its growth. The two types of particle probably emanated from different sources. The chromium-rich particles derived from either HK40 or austenitic stainless steels, while the iron carbide could have originated as oxide from mild or low alloy steel components. In summary, therefore, although in certain circumstances catalytic species were derived from spalled oxide trapped on the growing surface, it did not prove possible to establish the relative importance of the three potential sources.

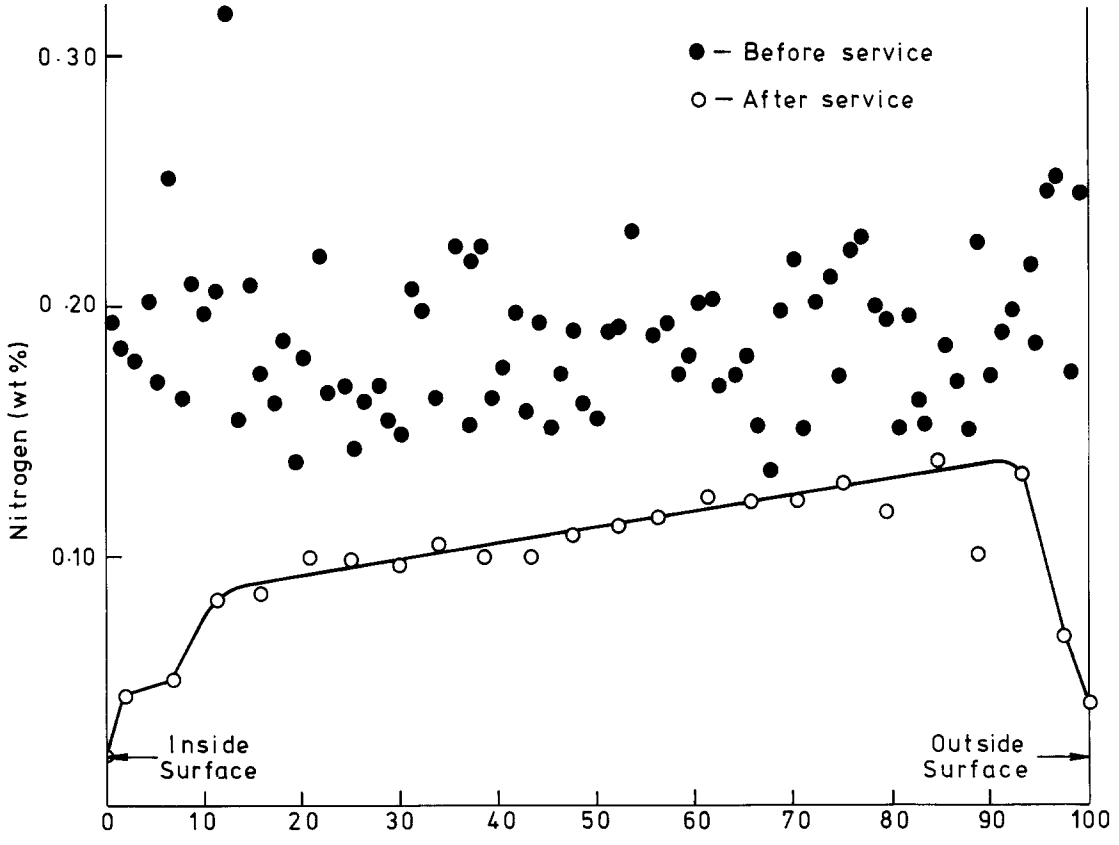

Figure 13 Nitrogen profiles across HK40 steel cracker tubes before and after service.

Sulphur compounds are well known inhibitors of carbonaceous deposition formed by heterogeneous reactions involving iron and nickel [10]. However, the effect of such poisons can be transitory if the sulphides thereby formed are oxidized by the environment. Sulphur was apparently associated in the deposit inner layer with nickel and iron and although it had not stopped deposit growth completely, it may have been effective to some degree. The sulphur originated either from the feedstock or was specifically introduced as a gas phase additive. The sources of the potassium chloride observed are not known nor is it clear what was its effect.

At a certain stage in the cracking cycle, growth of the inner layer stopped and was superseded by another process leading to the formation of the outer layer. At isolated regions, this second process was interrupted by the deposition of oxide particles, and metal catalysed deposit growth was resumed temporarily until it was again swamped by the second growth mechanism. In general the dense outer layer was characterized by radial and axial structural features. The columnar structure through the cross-section was both singly and continuously nucleated [11], while the deposit appeared to have been built up in a succession of discrete layers. This together with the low gas permeability of the deposit established that it formed by a heterogeneous process with outward growth at the deposit–gas interface and not at the inner interlayer interface. The concentrations of potentially catalytic metallic elements, such as iron and nickel, in the outer layer were extremely small. These elements were distributed fairly uniformly through the deposit and were not concentrated at the deposit–gas interface. In addition the form of the outer layer was completely different from that of the inner layer so that is is unlikely that a metal catalysed heterogeneous type mechanism was responsible for the outer layer formation. The small quantities of potentially catalytic metallic species and other inorganic impurities within the outer layer were either trapped dust particles or in the case, for example, of sulphur resulted from the degraddation on the deposit of appropriate compounds.

The outer layer was essentially a pyrocarbon,

but whose growth mechamism is not fully understood. Current theories seem to agree that the primary processes involve the decomposition of the hydrocarbon to form polynuclear aromatics. The theories then disagree as to whether these condense as droplets to undergo pyrolysis (dehydrogenation) on striking the substrate on which they solidify [12] or whether they are directly absorbed onto the tube walls and then decomposed [12, 13]. By comparison with the range of textures of the pyrocarbons produced on fuel particles [14], the production of the ordered layered structured ESC coke would appear to be more consistent with the latter mechanism, with the deposit surface being involved autocatalytically in the process of deposition [15].

Although it is believed that the main features of the deposit examined are representative of ESC pyrolysis tube coke formed from a naphtha feedstock, it must be recognised that there could be specific variations associated with the individual plant, its operating procedure and the hydrocarbon feedstock. This study has demonstrated the range of information that can be derived from characterization of plant deposits. The values of such studies are seen as providing a detailed understanding of the phenomena under all operating circumstances and confidence in coking alleviation procedures.

6. Conclusions

(1) Detailed physical and chemical characterization of a carbonaceous deposit formed on an HK40 steel ESC pyrolysis tube from a naphtha-steam feedstock showed that it consisted of two layers.

(2) The innermost layer (i.e. adjacent to the tube) was of variable thickness (20 μm to 1.5 mm) and was formed by heterogeneous reactions catalysed by iron and nickel. Enhanced deposition was linked with the presence of chromium-rich oxide particles which had been a source of catalytic species.

(3) The outer deposit layer was fairly uniform in thickness ($\sim$ 1 mm), had a columnar radial and axial layered structure, which together with the absence of any significant inorganic contaminants suggested it was formed by a similar autocatalytic growth mechanism as that for pyrocarbons.

(4) The attack of both the inner (cracker) and outer (hot-box) HK40 steel tube surfaces involved the formation of a chromium-rich adherent scale of variable thickness, a silicon-rich intergranular oxide and a zone of denuded chromium carbide and nitride particles beneath the oxide scale. The main differences in behaviour between the surfaces were that at the inner surface carburization and denitriding had also occurred beneath the carbide denuded zone. Carbon pick-up probably resulted from a crevice corrosion mechanism, while as a result of carburization chromium nitride was converted to the more stable chromium carbide.

Acknowledgements

This programme was sponsored by the Chemical and Minerals Requirements Board of the Department of Trade and Industry. We wish to thank Dr L. C. Dick, Dr B. Estruch and R. D. Smith (ICI Limited) for supplying the ESC coke sample and relevant plant information. We are grateful for the many detailed discussions during the course of this study we have had with them and their colleagues of Petrochemical and Agricultural Divisions, ICI, and also with Dr J. J. McCarroll (BP Research Centre). We gratefully acknowledge the experimental contributions to this study by Dr D. M. Poole, Dr H. E. Bishop, R. W. M. Hawes (EPMA), J. E. Bainbridge (SEM), B. L. Myatt (surface area measurement), M. D. Fones (X-ray diffraction), J. P. Jackson (HVEM), Dr J. P. Coad (XPS), J. Watling and E. H. Henderson (chemical analysis), J. W. McMillan and F. C. W. Pummery (nuclear microprobe analysis) and B. W. Ashton (RFL Springfields) (physical measurements). We also wish to thank Dr J. E. Antill for helpful discussions.

References

1. T. B. PIERCE, J. W. MCMILLAN, P. F. PECK and I. G. JONES, *Nucl. Instr. Methods* **118** (1974) 115.
2. C. OLIVIER, J. W. MCMILLAN and T. B. PIERCE, *ibid.* **124** (1975) 289.
3. L. A. ZEISS and E. HEINZ, *Chem. Eng. Prog.* **66** (1970) 68.
4. A. FERTILLO and B. PRINCIP, *Hydrocarbon Processing* **54** (1975) 174.
5. M. J. BENNETT, M. R. HOULTON, J. W. MCMILLAN, C. F. KNIGHTS, R. W. M. HAWES and F. C. W. PUMMERY, International Conference on the Behaviour of High Temperature Alloys in Aggressive Environments, Joint Research Centre, Pettern, The Netherlands, October, 1979.
6. R. T. K. BAKER, M. A. BARBER, F. S. FEATES, P. S. HARRIS and R. J. WAITE, *J. Catal.* **26** (1972) 51.
7. R. T. K. BAKER, P. S. HARRIS, R. B. THOMAS and R. J. WAITE, *ibid.* **30** (1973) 86.

8. T. BAIRD, J. R. FRYER and B. GRANT, *Carbon* **12** (1974) 591.
9. M. J. BENNETT, G. H. CHAFFEY, A. J. LANGFORD and D. R. V. SILVESTER, UK Atomic Energy Authority Report, AERE-R7407 (1973).
10. M. J. BENNETT, G. H. CHAFFEY, B. L. MYATT and D. R. V. SILVESTER, UK Atomic Energy Authority Report, AERE-R7408 (1973).
11. J. C. BOKROS in "Chemistry and Physics of Carbon", Vol. 5 edited by P. L. Walker Jr (Marcel Dekker, New York, 1969) p. 3.
12. J. LAHAYE, P. BADIE and J. DUCRET, *Carbon* **15** (1977) 87.
13. T. M. MUKHINA, G. L. STOLYAR, N. L. BARABANOV, B. S. BORDEN and N. P. SOLOMINA, *Sb. tr N11 Sintetich spirtov i organ prod* **5** (1974) 34.
14. H. J. PENKALLA, E. GYARMATI and H. NICKEL, Proceedings of the Fifth London International Carbon and Graphite Conference, September, 1978 (Society of the Chemical Industry) p. 835.
15. W. P. HOFFMAN, F J. VASTOLA and P. L. WALKER, Fourteenth Biennial Conference on Carbon, Pennsylvania State University, June 1979 (American Carbon Society) p. 139.

Received 17 January and accepted 30 June 1980.